Supplemental Information

Methods and Materials

Radiochemistry Synthesis of [^{11}C]PIB: PET imaging was accomplished using the radiotracer *N*-methyl-[^{11}C]2-(4'-methylaminophenyl)-6-hydroxybenzothiazole (chemically abbreviated as [^{11}C]6-OH-BTA-1 and referred to as simply [^{11}C]PIB). The preparation of [^{11}C]PIB and the precursor for the radiolabeling studies was carried out according to published literature (1). The radiochemical synthesis consists of three steps: (i) production of [^{11}C]CH_3I, (ii) incorporation of [^{11}C]CH_3I into the substrate, 2-(4'-aminophenyl)-6-methoxymethylbenzothiazole and (iii) deprotection of intermediate to give the final compound, [^{11}C]PIB.

PET Imaging: After obtaining written informed consent from the volunteer (and in the case of subjects with AD, a spouse or other family member also signed informed consent) the subject was positioned either in a Siemens 961 HR ECAT PET scanner (CTI, Knoxville KY) or in a Siemens 962 HR+ ECAT PET scanner (CTI, Knoxville KY). A catheter was placed in an antecubital vein. A transmission scan was obtained to correct attenuation. The room was darkened and noise minimized and the subject had their eyes closed during the scan. Simultaneous with intravenous injection of 4 - 20 mCi (mean = 11 mCi) of [^{11}C]PIB, a 60 minute dynamic PET scan in 3D mode (septa retracted) was initiated (24 x 5 sec frames; 9 x 20 sec frames; 10 x 1 min frames; 9 x 5 min frames) (2).

Data Processing: Dynamic PET images were reconstructed with the measured attenuation factors and a ramp filter (final image resolution approximately 5 mm full-width half-maximum, or FWHM). Scatter correction using a fully 3D single scatter simulation algorithm was performed (3). PET-MR within-participant alignment was performed using an in-house cross-modal registration algorithm that minimizes the error function calculated from voxel-by-voxel activity levels, similar to maximizing the

correlation matrixes (3-4). See (5-6) for more details and prior use; procedures are similar to (7). This algorithm emphasizes image gradient and is thus robust for cross-modal data alignment. Within the dynamic PET data, head motion was corrected using the cross-modal alignment, rather than the intramodal alignment, due to the dramatic changes in tissue activity distribution during the scanning time. Alignment to an atlas target was accomplished by registration of each individual participant's structural MRI image to an atlas target (8) that minimizes bias due to atrophy (4). Alignment of the PET data was then computed using matrix multiplication resulting in an atlas-transformed, PET image resampled to 1 mm isotropic voxels. Registration was visualized in each participant to verify proper alignment. In addition to the individual dynamic frames, smoothed (to approximately 9mm FWHM), aligned and summed images of the data using frames from 0 to 15 minutes and from 30 to 60 minutes after injection were created in atlas space for each subject for visual inspection.

Regions of Interest: Three-dimensional regions of interest (ROIs) were created for each subject based on their individual MRI as previously described (2). The mean cortical binding potential (MCBP) was created as previously described (2) from the average of the binding potential (BP) values in the precuneus, lateral temporal cortex, gyrus rectus, and prefrontal cortex regions. We used the image processing software ANALYZE (Mayo Clinic) to draw each ROI on the individual's MPRAGE MRI image. ROI time-activity curves were generated by applying the MRI-derived three-dimensional ROIs to the high resolution (unblurred) coregistered dynamic PET data. The ROIs were used to extract PIB activity profiles using the unblurred (ramp filtered) PET images. Logan graphical analysis (9) was then applied to calculate the distribution volume (DV) and binding potential (BP = DV -1) for statistical analyses. Subjects with a MCBP ≥ 0.18 were defined as PIB+; those with MCBP < 0.18 were defined as PIB- (10).

Structural MRI: All subjects underwent MRI scanning in a 3T Siemens TRIO system (Erlangen, Germany) at the Research Imaging Center of the Mallinckrodt Institute of Radiology, Washington University Medical School. Structural imaging sessions began with acquisition of a scout scan with three orthogonal slices, followed by a coarse 3D sagittal T1-weighted MP-RAGE used to automatically compute fMRI slice tilts and offsets that optimize whole brain coverage parallel to the AC-PC plane. This computation ("pre-registration") standardizes the fMRI coverage across subjects and provides highly reproducible slice positioning in longitudinal studies. High-resolution structural images were acquired using a 3D sagittal T1-weighted MP-RAGE acquisition optimized for contrast-to-noise ratio and resolution (11) [TE=16ms, TR=2400ms, TI=1000ms, flip angle=8^{o}, 256x256 acquisition matrix, 1x1x1 mm voxels]. The high resolution MP-RAGE was used for definitive atlas registration. High-resolution 2D multislice oblique axial spin density/T2-weighted fast spin echo (FSE) structural images were acquired using slice tilts and positions computed by slice preregistration [TE=455ms, TR=3200ms, 256x256 acquisition matrix, 1 acquisition, 1x1x1 mm voxels]. The T2-weighted FSE data was used in the fMRI atlas registration procedure.

fMRI Scanning Methods: The functional images were collected in runs using a gradient spin-echo sequence (TE=27ms, TR=384ms, FOV=256mm, flip angle=90°) sensitive to blood oxygenation level-dependent (BOLD) contrast (T2* weighting). 36 contiguous, 4.0 mm thick slices were acquired parallel to the anterior-posterior commissure plane (4.0 mm approximately isotropic voxels) providing complete brain coverage. Two fMRI runs included 164 volumes each, continuously acquired at a TR of 2.2 sec (6 minutes each). MR data was reconstructed into images, and then normalized across runs by: 1) scaling whole-brain signal intensity to a fixed value; and 2) removing the linear slope on a voxel-by-voxel basis to counteract effects of drift (12). The MR data was aligned to correct for head motion using a six-parameter rigid-body rotation and translation correction which mutually registers all frames in all runs

for each subject (13; 3; 7). Between-subjects analyses were conducted after transformation of the data to a common atlas space and then the images were blurred with an 8mm FWHM Gaussian filter. The transforms were combined by matrix multiplication so that reslicing of data in conformity with the atlas involved only one interpolation.

Quality Assurance: To determine the comparability of movement across populations we conducted quality checks and compared between the subject groups. The mean movement in mm for the combined x, y and z axis was determined for each group, based on analysis of head position rigid body translation and rotation. The data derived from the adjustments needed to realign head movement on a frame-by-frame basis were calculated as root mean square (RMS) values for translation and rotation in the x, y and z planes in millimeters. For the AD vs PIB- comparison the mean and SD were 0.56 (0.23) and 0.50 (0.27), respectively, $p > .05$. For the PIB+ and PIB- comparison the mean and SD were 0.40 (0.18) and 0.43 (0.19), respectively, $p > .05$.

Functional Connectivity Analysis of Resting State Activity: We used standard methods for the analysis (14-18). See (14) for a more detailed description. In preparation for functional connectivity analysis, the BOLD volumetric time series were concatenated and passed through several additional pre-processing steps: 1) spatial smoothing; 2) temporal filtering retaining frequencies in the 0.009-0.08 Hz band; and 3) removal by regression of several sources of variance. Temporal derivatives of these regressors were included in the linear system, thereby accounting for the time-shifted versions of spurious variance (e.g., delayed whole brain BOLD signal in venous structures). Correlation maps were produced by extracting the BOLD time course from the precuneus seed region, then computing the correlation coefficient between that time course and the time course from all other brain voxels. The principal techniques are: 1) measurement of regional BOLD fluctuation power; 2) measurement of inter-regional (ROI-ROI) covariance and correlation; and 3) computation of whole brain, voxel-wise intrinsic

functional connectivity maps. Each fMRI run thus provides a series of BOLD signal measurements at each voxel within the field of view. The present main results (regional functional connectivity) were obtained by computing Pearson correlation coefficients (r) for region pairs. Statistical tests on regional FC results were computed after application of Fisher's z transform ($z = 0.5Ln[(1+r)/(1-r)]$), which yields variates that are approximately normally distributed.

Testing of Functional Correlations During Resting State Activations: Significance maps for fixed effects inference are created for each individual by converting the Fisher z values to z scores (i.e. zero mean, unit variance, Gaussian distributions) by dividing by the square root of the variance, computed as $1/\sqrt{(n-3)}$ where n is the degrees of freedom in the measurement. Since individual time points in the BOLD signal are not statistically independent, the degrees of freedom must be corrected according to Bartlett's theory, i.e. computing the integral across all time of the square of the autocorrelation function (19). These single subject Z score maps are used in computing the spatial correlation coefficient. Group difference significance maps were created using a random effects analysis on the individual Fischer z transformed correlation maps for all subjects.

As described in the Methods section, we first conducted unpaired t-tests comparing Alzheimer's disease and half of the PIB- sample. The resulting unpaired t values were converted to z scores and thresholded using $p < 0.05$, two-tailed ($z = 1.96$), for hypothesis generation. This data is shown in Figure S1. Then, as described in the Methods section an independent sample of 24 PIB- subjects was compared with PIB+ subjects (see Figure 1 in main text).

Correlation between PIB BP and Precuneus Resting State Connectivity in the PIB+ Group: To determine whether the observed resting state differences in connectivity in the PIB+ group could be explained by elevations of amyloid binding in the precuneus we conducted correlations in the PIB+ group between the BP in the precuneus and its connectivity with each of the target regions

demonstrating resting state connectivity differences. The correlations (Pearson's product moment, r) were as follows: anterior cingulate (AC) = .13, left hippocampus (L hip) = -.16, left parahippocampus (L parahip) = -.07, visual cortex (VC) = -.10, dorsal cingulate (DC) = .26, gyrus rectus (GR) = -.25, superior precuneus (Sup PC) = -.18. None of these was significant, all $p > 0.05$.

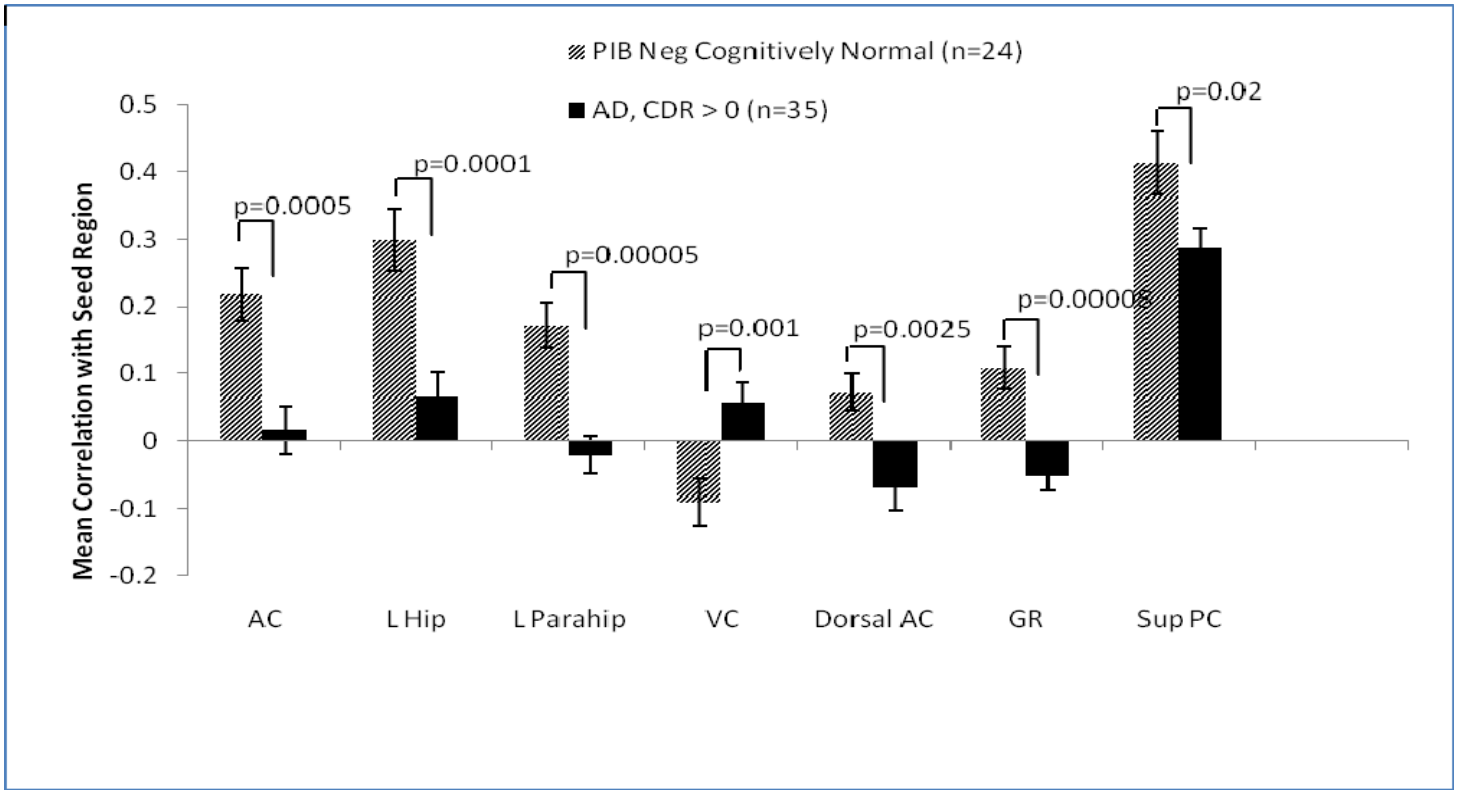

Figure S1. Altered Functional Connectivity to the Precuneus in Alzheimer's Disease Participants vs PIB- Cognitively Normal Participants.

The graph compares regional correlation magnitudes for AD and PIB- individuals in half of the PIB- subjects, used for hypothesis generation. The regions identified as differing in resting state functional connectivity of the precuneus were in visual cortex (VC) (both L and R), L hippocampus (L hip), L parahippocampus (L parahip) , L anterior cingulate (AC), L and R gyrus rectus (GR), dorsal anterior cingulate (Dorsal AC) and superior precuneus (Sup PC) regions.

1. Mathis CA, Wang Y, Holt DP, Huang GF, Debnath ML, Klunk WE (2003): Synthesis and evaluation of 11C-labeled 6-substituted 2-arylbenzothiazoles as amyloid imaging agents. *J Med Chem* 46: 2740-2754.

2. Mintun MA, Larossa GN, Sheline YI, Dence CS, Lee SY, Mach RH, *et al*. (2006): [11C]PIB in a nondemented population: potential antecedent marker of Alzheimer disease. *Neurology* 67: 446-452.

3. Snyder AZ (1996): Difference image vs ratio image error function forms in PET-PET realignment. In: Myer R, Cunningham VJ, Bailey DL, Jones T, eds. *Quantification of Brain Function Using PET*. San Diego: Academic Press, 131-137.

4. Buckner RL, Head D, Parker J, Fotenos AF, Marcus D, Morris JC, *et al*. (2004): A unified approach for morphometric and functional data analysis in young, old, and demented adults using automated atlas-based head size normalization: reliability and validation against manual measurement of total intracranial volume. *Neuroimage* 23: 724-738.

5. Accorsi R, Adam LE, Werner ME, Karp JS (2004): Optimization of a fully 3D single scatter simulation algorithm for 3D PET. *Phys Med Biol* 49: 2577-2598.

6. Woods RP, Cherry SR, Mazziotta JC (1992): Rapid automated algorithm for aligning and reslicing PET images. *J Comput Assist Tomogr* 16: 620-633.

7. Woods RP, Mazziotta JC, Cherry SR (1993): MRI-PET registration with automated algorithm. *J Comput Assist Tomogr* 17: 536-546.

8. Talairach J, Tournoux P (1998): *Co-planar Stereotaxic Atlas of The Human Brain*. New York: Thieme Medical.

9. Logan J, Fowler JS, Volkow ND, Wang GJ, Ding YS, Alexoff DL (1996): Distribution volume ratios without blood sampling from graphical analysis of PET data. *J Cereb Blood Flow Metab* 16: 834-840.

10. Roe CM, Mintun MA, D'Angelo G, Xiong C, Grant EA, Morris JC (2008): Alzheimer's and cognitive reserve: education effect varies with [11C]PIB uptake. *Arch Neurol* 65: 1467-1471.

11. Epstein FH, Mugler JP 3rd, Brookeman JR (1994): Optimization of parameter values for complex pulse sequences by simulated annealing: application to 3D MP-RAGE imaging of the brain. *Magn Reson Med* 31: 164-177.

12. Bandettini PA, Jesmanowicz A, Wong EC, Hyde JS (1993): Processing strategies for time-course data sets in functional MRI of the human brain. *Mag Res Med* 30: 161-173.

13. Friston KJ, Jezzard P, Turner R (1994): The analysis of functional MRI time series. *Hum Brain Mapp* 1: 153-171.

14. Fox MD, Snyder AZ, Vincent JL, Corbetta M, Van Essen DC, Raichle ME (2005): The human brain is intrinsically organized into dynamic, anticorrelated functional networks. *Proc Natl Acad Sci USA* 102: 9673–9678.

15. Fox MD, Corbetta M, Snyder AZ, Vincent JL, Raichle ME (2006): Spontaneous neuronal activity distinguishes human dorsal and ventral attention systems. *Proc Natl Acad Sci USA* 103: 100046–100051.

16. Fox MD, Raichle ME (2007): Spontaneous fluctuations in brain activity observed with functional magnetic resonance imaging. *Nat Rev Neurosci* 8: 700–711.

17. Vincent JL, Snyder AZ, Fox MD, Shannon BJ, Andrews JR, Raichle ME, *et al*. (2006): Coherent spontaneous activity identifies a hippocampal-parietal memory network. *J Neurophys* 96: 3517–3531.

18. Vincent JL, Kahn I, Snyder AZ, Raichle ME, Buckner RL (2008): Evidence for a frontoparietal control system revealed by intrinsic functional connectivity. *J Neurophys* 100: 3328-3342.

19. Jenkins GM, Watts DG (1968): *Spectral Analysis and its Applications*. Boca Raton, FL: Emerson-Adams.